



An Efficient AC Drive Scheme for Electric Vehicles

E. Elbakush¹, A. M. Sharaf²

Electrical and Computer Engineering, University of New Brunswick, Fredericton, NB, Canada¹
Sharaf Energy Systems, Inc., Fredericton, NB, Canada²

Abstract: This paper presents an efficient stabilized AC Drive-Switched Capacitor Filter Compensation Scheme (SFC) for an electric vehicle (EV) using a squirrel-cage induction motor. The dynamic modelling and coordinated control strategy for the integrated-DC side switched filter-compensation scheme (SFC) with energy-recovery is fully validated for a hybrid power supply using a Lithium-Ion battery and fuel cell (FC) on the DC side with a 6-pulse VSI-inverter fed Induction motor drive. The integrated DC/AC Induction motor drive is stabilized using a hybrid SFC that ensures a fully stabilized DC Bus voltage with reduced inrush current conditions under DC side supply source and load excursions. The Lithium-Ion battery and fuel cell sources are utilized efficiently using a novel multi regulator, error driven and multi loop control strategy. The hybrid switched filter compensator is equipped with a tri-loop weighted modified PID (WMPID) controller to ensure full DC Bus stabilization and minimal inrush current conditions as well as energy recovery under deceleration and load excursions. The paper presents the validation of the DC side filter-compensation scheme and coordinated control strategy for the AC voltage source inverter using decoupled torque and flux loops of the three-phase squirrel-cage induction motor. The AC Induction motor is controlled by the first controller for different operating conditions using the direct torque control (DTC) technique, while the second controller is used to stabilize the DC common Bus and ensure energy recovery with minimal inrush current conditions. The unified DC-AC Drive system is modelled using MATLAB/Simulink/ Sim-power software environment.

Keywords: EV-AC Drive, Hybrid Fuel Cell and Lithium-Ion Battery, Switched Filter Compensator (SFC).

I. INTRODUCTION

Electric vehicles (EVs) are emerging as a viable economical alternative to ICE fuel based transportation systems as an elegant step to reduce pollution and Green House Gases (GHG) and reduce smog and air quality, hence reduce environmental problems created by internal combustion engines. Besides energy-utilization efficiency and reduction in vehicle emissions, EV can be charged by renewable energy sources such as photovoltaic solar and wind schemes. Among current limitations of EVs is low energy density and required long charging time for the present batteries [1]. Therefore, optimal energy utilization, energy recovery and efficient electrical energy/power management is very important in EV-DC and AC drive designs; in addition optimal design of the AC motor for weight, volume and operating maximum efficiency at full rated condition is needed by proper selection of the unified DC-AC drive components as well as optimal control strategies. Desired features of the propulsion system (AC motor) for an EV are high ratios of resultant driving torque/inertia and power/volume and weight, starting and maximum torque capabilities and accelerating torque levels are also crucial (300-400%), high speed, low level of audible noise, low maintenance, small size, low weight, reasonable cost, high efficiency over low and high speed ranges, energy recovery on braking, and non-sensitivity to acceleration forces. Squirrel-cage induction motors have most of the above- mentioned features [2]. Recently, the increasing limitations imposed on the exhaust emissions from internal combustion CNG/gasoline and diesel powered engines and the traffic restrictions in the urban areas have given a strong impulse toward the development of electrical propulsion systems for automotive applications. The hybrid electric vehicle comprises the motor drive comprising of AC drive motor, a 6-pulse-VSI-power converter, speed controller, DC Bus stabilizing filter/switched capacitor and dynamic controller to ensure energy recovery and efficient energy utilization. Different types of AC motors have been proposed for use in EVs; separately excited synchronous motors, different reluctance motors, different permanent magnet motors and Induction motors. For this drive system a squirrel-cage induction motor is chosen due to mature technology, high reliability, high efficiency even in the high-speed range and



International Journal of Advanced Research in Electrical, Electronics and Instrumentation Engineering

(An ISO 3297: 2007 Certified Organization)

Vol. 2, Issue12, December 2013

low production cost [3]. Many control techniques have been applied on squirrel-cage Induction motors [4], [5]. The two well-known AC Induction motor control methods are based on decoupled field-oriented control (FOC) and direct torque control (DTC). Hybrid FOC-DTC method utilizes the advantages of the both FOC and DTC methods and at the same time eliminates the extra required hardware and control estimation cost and complexities. So it appears to be very suitable for EV applications. As DTC, the required measurements for this control technique are only the input currents. Flux, torque, and speed are estimated. A loss- minimization strategy is associated with the hybrid method to maximize the drive efficiency. Moreover, a speed estimation process and a robust flux weakening strategy are proposed and applied to the basic drive system to make it more proper for EV applications [6-7].

Induction motor has many advantages compared to DC motor, synchronous motor and switched reluctance motor in many aspects, such as controllability, reliability, technological, maturity and cost as indicated by recent comparative study for hybrid electric vehicles (HEV) [3], [4], [8]. Therefore, induction motor is one of the right electric motor candidates for automotive applications.

Induction motors have found the primal use in all industrial applications due to their simple construction, ruggedness, low cost, reliability, and no need for maintenance. Fast torque response and high efficiency variable speed drives are very attractive for some special application fields that fed by limited power supply, such as electric vehicle, aerospacecraft and so on. High dynamic performance of induction motor drives is indispensable in many applications of today's automatically controlled machines. Induction motor control has attracted much attention recently in the power electronics field. Field-oriented control has been developed, enabling an ac motor to attain dynamic responses as rapid as for dc motor. The principle of field-oriented vector control is based on Fleming's law, which describes the interaction force between fluxes and currents. Many papers have reported the problems associated with compensating various parameters. The current-controlled inverters typically used in the field-oriented drive system develop output waveforms, which do not compare favourably with those of the voltage- controlled inverter. The current controlled inverter often causes increased motor harmonic losses and acoustic noise during steady-state operation [9], [10], [11].

DTC is a suitable technology for high-performance electric drive systems. Simple algorithms, fast dynamic response and strong robustness to parameter variation and load disturbance characterize it. Therefore, the method combined DTC with a loss minimization approach will not only guarantee fast torque dynamic response of EV, but also maximize operating efficiency of that [12], [13], [14]. Many control techniques have been applied on squirrel-cage induction motors [15], [16], [17], [18], [19], [9]. Among these techniques, DTC [17], [18], [9], [20] appears to be very convenient for EV applications. The required measurements for this control technique are only the input currents. Flux, torque, and speed are estimated. The input of the motor controller is the reference speed, which is directly applied by the pedal of the vehicle [7].

The main objective of this paper is to design an efficient-well stabilized EV-AC drive scheme for AC induction motor used for EV using a novel switched filter-compensation scheme and dynamic control strategies for a hybrid fuel cell Lithium-Ion battery source. The fuel cell can be used as an additional back-energy source for hybrid EV. The self-regulating controller is proposed based on weighted modified proportional integral derivative (WMPID) algorithm. The switched filter compensator is controlled by tri-loop error-driven regulators to operate at tracking any reference speed trajectory under varying parameter and load conditions. The control system comprises four different regulators to track speed reference trajectory with minimum over/under current, inrush, ripple conditions. Time descaled and decoupled multi loop control scheme has been validated for effective dynamical speed reference trajectory tracking, efficient power utilization, limited inrush current conditions and reduced DC side transients and voltage excursions.

II. SAMPLE STUDY SYSTEM

Figure (1) shows the proposed EV-AC induction motor drive scheme with the Lithium-Ion battery and FC. The proposed drive system consists of five parts. There are DC voltage supplies like a Lithium-Ion battery, FC, switched filter compensator (SFC), a controlled four IM motors for wheels, a freewheel diode, and DC load. The DC/AC compensator scheme is used to ensure stable, efficient, minimal inrush operation of the hybrid renewable energy scheme. The WMPID regulator and coordinated controller are used for the following purposes:

- 1) The IM motor drive with the speed reference tracking regulator that ensure speed reference tracking with minimum inrush conditions and ensure reduced voltage transients and improved energy utilization.

International Journal of Advanced Research in Electrical, Electronics and Instrumentation Engineering

(An ISO 3297: 2007 Certified Organization)

Vol. 2, Issue12, December 2013

- 2) Hybrid switched filter compensator (SFC) regulator is connected to pulse width modulated (PWM) switching scheme to regulate the DC Bus voltage and minimize inrush current transients and load excursions. The SFC device acts as a matching DC/DC interface device between the DC load dynamic characteristics.

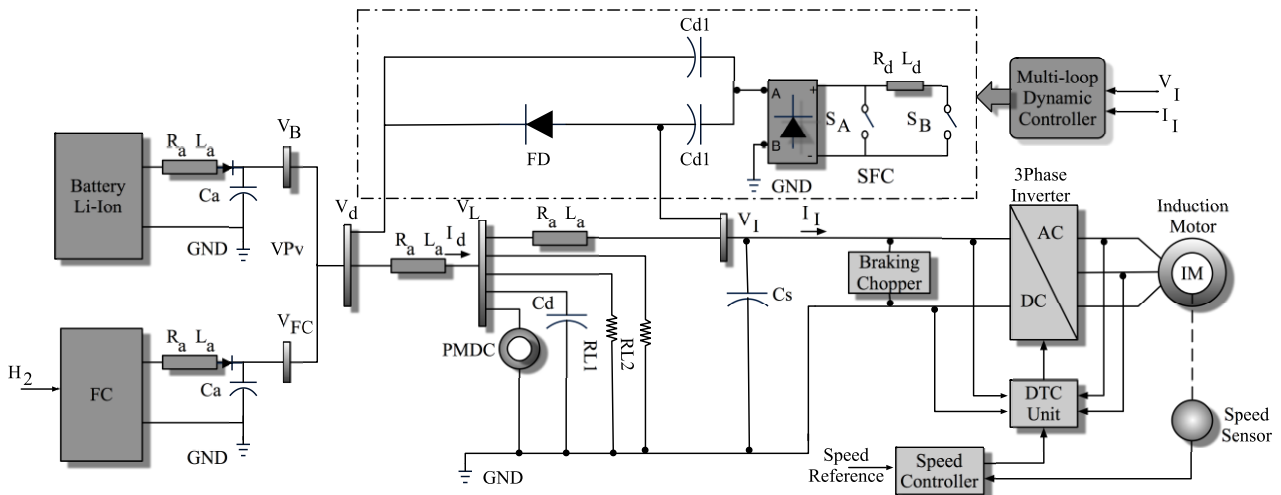


Fig. 1 The proposed AC Induction Motor electric vehicle drive system with Switched Filter Compensation Scheme

A. Induction Motor-Model

The mathematic model of an induction motor in the stator-flux fixed frame, in which stator current vector and stator flux vector act as state variables can be described by:

$$\dot{\vec{i}}_s = -\frac{1}{\sigma L_s} \left[R_s - j\sigma L_s (\omega_e - p\omega_r) + \frac{R_r L_s}{L_m} \right] \vec{i}_s - \frac{1}{\sigma L_s} \left[j(2\omega_e - p\omega_r) - \frac{R_r}{L_m} \right] \vec{\Psi}_s + \frac{1}{\sigma L_s} \vec{v}_s \quad (1)$$

$$\dot{\vec{\Psi}}_s = -R_s \vec{i}_s - j\omega_e \vec{\Psi}_s + \vec{v}_s \quad (2)$$

$$T_e = \frac{3p}{2} \vec{i}_s \times \vec{\Psi}_s \quad (3)$$

where:

$$\vec{v}_s = \begin{bmatrix} v_{sd} & v_{sq} \end{bmatrix}^T : \text{vector of stator voltages}$$

$$\vec{i}_s = \begin{bmatrix} i_{sd} & i_{sq} \end{bmatrix}^T : \text{vector of stator currents}$$

$$\vec{\Psi}_s = \begin{bmatrix} \Psi_{sd} & \Psi_{sq} \end{bmatrix}^T : \text{vector of stator fluxes}$$

$$\vec{\Psi}_r = \begin{bmatrix} \Psi_{rd} & \Psi_{rq} \end{bmatrix}^T : \text{vector of rotor fluxes}$$

$$S = 1 - \frac{L_m}{L_r L_s} : \text{leakage induction factor}$$



International Journal of Advanced Research in Electrical, Electronics and Instrumentation Engineering

(An ISO 3297: 2007 Certified Organization)

Vol. 2, Issue12, December 2013

R_s, R_r : stator and rotor resistance

L_s, L_r : stator and rotor inductance

L_m : mutual induction

W_e, W_r : stator flux vector and rotor speed

p : number of pole pairs

T_e : electromagnetic torque

\wedge : cross product

From (1), (2) and (3) it can be modified as following

$$\dot{x}_1 = -a_1x_1 - a_2x_2 + a_3x_3 + a_4x_4 + bv_d \quad (4)$$

$$\dot{x}_2 = a_2x_1 - a_1x_2 - a_4x_3 + a_3x_4 + bv_q \quad (5)$$

$$\dot{x}_3 = -a_5x_1 + a_6x_4 + v_d \quad (6)$$

$$\dot{x}_4 = -a_5x_2 - a_6x_3 + v_q \quad (7)$$

$$T_e = \frac{3p}{2} (x_2x_3 - x_1x_4) \quad (8)$$

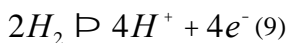
The state vector $x = [x_1, x_2, x_3, x_4]^T = [i_{sd}, i_{sq}, Y_{sd}, Y_{sq}]^T$, the control vector $U = [v_d, v_q]^T$ the output vector

$Y = [x_1, x_2]^T = [i_{sd}, i_{sq}]^T$, and the parameters $a_1 = \frac{R_s}{SL_s} + \frac{R_r}{SL_m}$, $a_2 = W_e - pW_r$, $a_3 = \frac{R_r}{SL_s L_m}$,

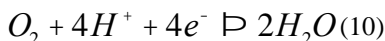
$a_4 = \frac{(2W_e - pW_r)}{SL_s}$, $a_5 = R_s$, $a_6 = W_e$, and $b = \frac{1}{SL_s}$.

B. Fuel Cell Energy System Model

Fuel cells are electrochemical devices that convert the chemical energy of a gaseous fuel directly into electricity and are widely regarded as a potential alternative stationary and mobile power source. FC stack systems are under intensive development by several manufacturers, with the Polymer Electrolyte Membrane (PEM) FCs currently considered by many to be in a relatively more developed stage for ground vehicle applications. Fuel cell stacks were connected in series/parallel combination to achieve the rating desired. A fuel cell consists of an electrolyte sandwiched between two electrodes. The electrolyte has a special property that allows positive ions (protons) to pass through while blocking electrons. Hydrogen gas passes over one electrode, called an anode, and with the help of a catalyst, separates into electrons and hydrogen protons.



The protons flow to the other electrode, called a cathode, through the electrolyte while the electrons flow through an external circuit, thus creating electricity. The hydrogen protons and electrons combine with oxygen flow through the cathode, and produce water.



The overall reaction of the fuel cell is therefore



The voltage produced from one cell is between 0 to 1 volts depending on fuel cell operating conditions and the size of load connected to the fuel cell. The typical value of the fuel cell voltage is about 0.7 volts. To get higher voltage, multiple cells are stacked in series. The total stack voltage is the number of cells multiplied by the average cell voltage. Like other electrical devices, there are electrical resistances in the fuel cell [21]. Figure (2) shows FC reaction.

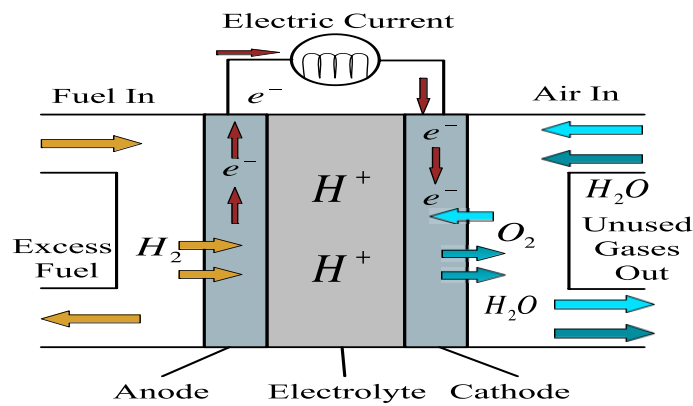


Fig. 2 Fuel cell reaction.

C. Lithium-Ion Battery Energy System Model

The construction of lithium-ion battery includes a negative electrode, a positive electrode, separator between the electrodes, and electrolyte for submerging the electrodes. The negative electrodes is made of active materials including at least one lowly graphitized carbon material and least one highly graphitized carbon material. The positive electrode made of active materials including lithium ion, transition metal ion and polyanion [3]. The lithium-ion battery is chosen to be the best because it is one of the best energy density, no memory effect, long life cycle and slow loss of charge.

III. CONTROL STRATEGIES

A. Weighted Modified Proportional Integral Derivative

The proposed tri-loop error driven Weighted Modified Proportional Integral Derivative (WMPID) controller and shown in Figure (3), is a novel advanced regulator concept that operates as an adaptive dynamic type multi-purpose controller capable of handling sudden parametric changes and load and /or source excursions. By using the tri-loop error driven WMPID controller, it is expected to have a smoother, less dynamic over-shoot, fast and more robust speed controller when compared to those of classical control schemes. The dynamic supplementary control loops utilizes the (per-unit) three dimensional-error vector ($e_{v_i}, e_{I_i}, e_{p_i}$) governed by the following equations:

$$e_{v_i}(k) = 1 - \left(\frac{V_i(k)}{V_i \text{ Base}} \right) \cdot \left(\frac{1}{1 + ST_1} \right) (12)$$

$$e_{I_i}(k) = \left(\left(\frac{I_i(k)}{I_i \text{ Base}} \right) \cdot \left(\frac{1}{1 + ST_1} \right) \right) \cdot \left(\left(\frac{1}{1 + SD} \right) - 1 \right) (13)$$

$$e_{p_i}(k) = \left(\left(\frac{V_i(k)}{V_i \text{ Base}} \right) \cdot \left(\frac{I_i(k)}{I_i \text{ Base}} \right) \cdot \left(\frac{1}{1 + ST_2} \right) \cdot \left(\left(\frac{1}{1 + SD} \right) - 1 \right) \right) (14)$$

International Journal of Advanced Research in Electrical, Electronics and Instrumentation Engineering

(An ISO 3297: 2007 Certified Organization)

Vol. 2, Issue12, December 2013

Moreover, the total or global error $e_{Total}(k)$ for the DC side SFC scheme at a time instant:

$$e_{Total}(k) = g_{V_i} \times e_{V_i}(k) + g_{I_i} \times e_{I_i}(k) + g_{P_i} \times e_{P_i}(k) \quad (15)$$

The system control voltage has the following form in the time domain:

$$V_c(t) = K_p \times e(t) + K_i \int_0^t e_i \times dt + K_d \frac{de_i(t)}{dt} + g_1 \times (e_i(t))^2 + g_2 \times (e_i(t) - e_i(t - t)) \quad (16)$$

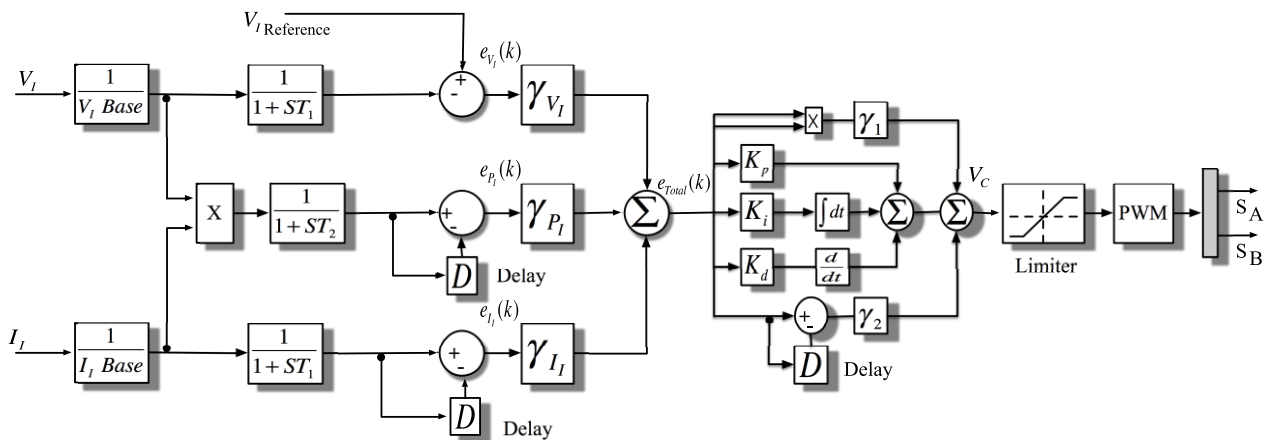


Fig. 3 Tri-loop error driven weighted modified PID dynamic controller for the SFC.

B. Speed Control of the Induction Motor

PI regulator for direct torque control is considered as one of robust control for induction motor, its practical implementation is easy in comparison with other techniques. Figure (4) represents the speed response in the case of a variation, and inversion of speed applied to the using a classic PI regulator. The speed controller is based on the PI regulator. The output of this regulator is a torque set point applied to the DTC controller. The Direct Torque and Flux Control (DTC) controller contains five main blocks as shown in the Figure (4). The Torque & Flux calculator is used to estimate the motor flux $\alpha\beta$ components and the electromagnetic torque. This calculator is based on motor equation synthesis. The $\alpha\beta$ vector block is used to find the sector of the $\alpha\beta$ plane in which the flux vector lies. The Flux & Torque Hysteresis blocks contain a two-level hysteresis comparator for flux control and a three-level hysteresis comparator for the torque control. The Switching table block contains two lookup tables that select a specific voltage vector in accordance with the output of the Flux & Torque Hysteresis comparators [13].

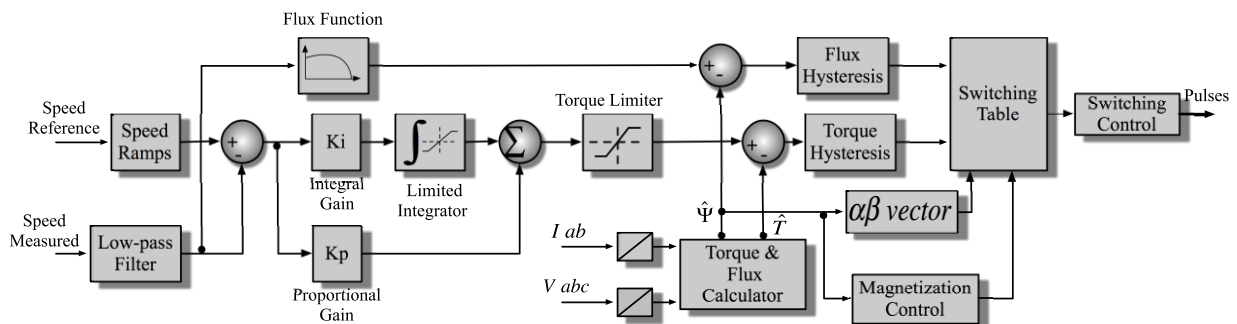


Fig. 4 Speed-tracking controller is based on a Proportional plus Integral-PI regulator.

International Journal of Advanced Research in Electrical, Electronics and Instrumentation Engineering

(An ISO 3297: 2007 Certified Organization)

Vol. 2, Issue12, December 2013

IV. DIGITAL SIMULATION RESULTS

The Lithium-Ion and FC driven three-phase squirrel-cage induction motor is used as a propulsion system of EV performance is compared for two test cases, namely open circuit fault and short circuit fault at common DC Bus. The weighted modified PID has been applied to the voltage and current-tracking control of the Lithium-Ion and FC driven scheme for performance comparison. MATLAB/Simulink software was used to design, test and validate the effectiveness of the scheme without and with the SFC device. The digital dynamic simulation model using MATLAB/Simulink software environment allows for low-cost assessment and prototyping, system parameters selection and optimization of control settings. The use of weighted modified PID algorithm is used for gain adjusting to minimize controller absolute value of total error. This is required before full-scale prototyping, which is both expensive and time-consuming. The effectiveness of dynamic simulators brings on detailed sub-models selections and tested sub-models MATLAB library of power system components already tested and validated. The control system comprises the three dynamic multi-loop error-driven regulators and is coordinated to minimize the selected objective functions.

Figure (5) shows the performance of the drive in a wide speed range. At time $t = 0$ s, the speed set point is 400 rpm. As shown in the figure, the speed precisely follows the acceleration ramp. At $t = 0.5$ s, the nominal load torque is applied to the motor. At $t = 0.5$ s, the speed set point is changed to 0 rpm. The speed decreases to 0 rpm. Figure (6) shows the performance of the drive in a wide speed range. At time $t = 0$ s, the speed set point is 500 rpm. As shown in the following figure, the speed precisely follows the acceleration ramp. At $t = 0.5$ s, the nominal load torque is applied to the motor. At $t = 1$ s, the speed set point is changed to 0 rpm. The speed decreases to 0 rpm. At $t = 1.5$ s., the mechanical load passes from 792 N.m to -792 N.m. Figures (7, 8) show the stator current and DC Bus voltage response during different operation modes. Digital simulation for the EV-IM drive scheme shows the voltage and the current for the system without SFC, with SFC with Freewheel diode. Figures (9, 10, 11, 12, 13) show the system dynamic voltage, current and response at all Buses. In the same time, Figures (14, 15, 16, 17, 18, 19, 20, 21, 22, 23) show the system dynamic voltage, current and response at all Buses under open circuit and short circuit fault condition at VD Bus respectively. Figure (24) shows the performance of the drive in a wide speed range under short circuit fault at AC Bus. Figure (25) shows the stator current and DC Bus voltage response under short circuit fault at AC Bus.

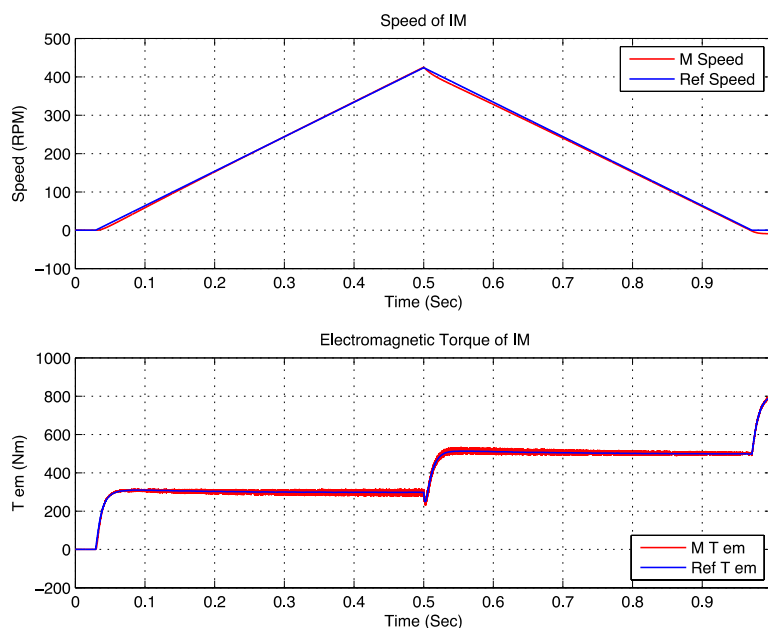


Fig. 5 Motor response during different operation modes.

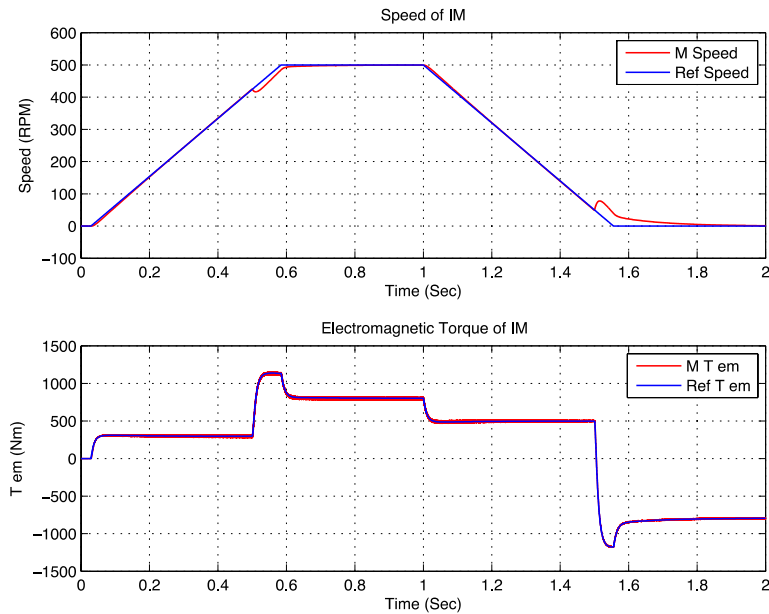


Fig. 6 Motor response during different operation modes.

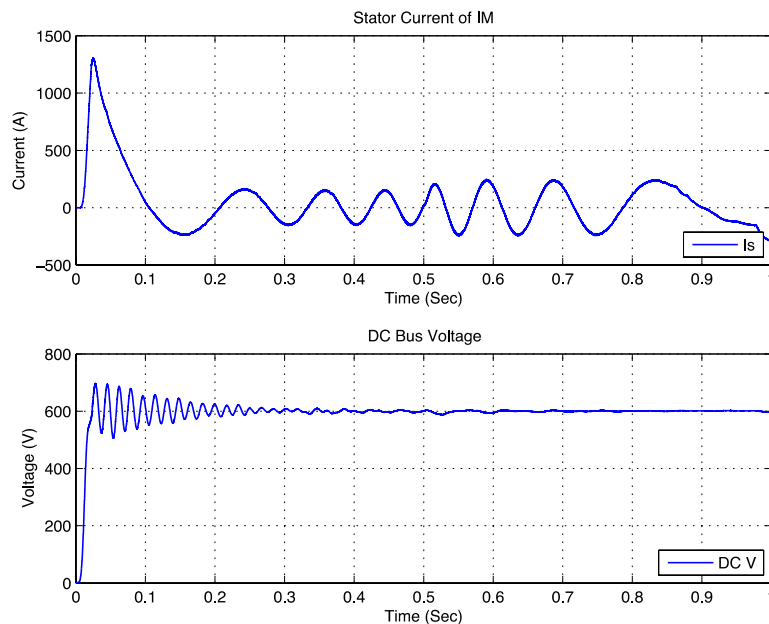


Fig. 7 Stator current and DC Bus voltage response during different operation modes.

International Journal of Advanced Research in Electrical, Electronics and Instrumentation Engineering

(An ISO 3297: 2007 Certified Organization)

Vol. 2, Issue12, December 2013

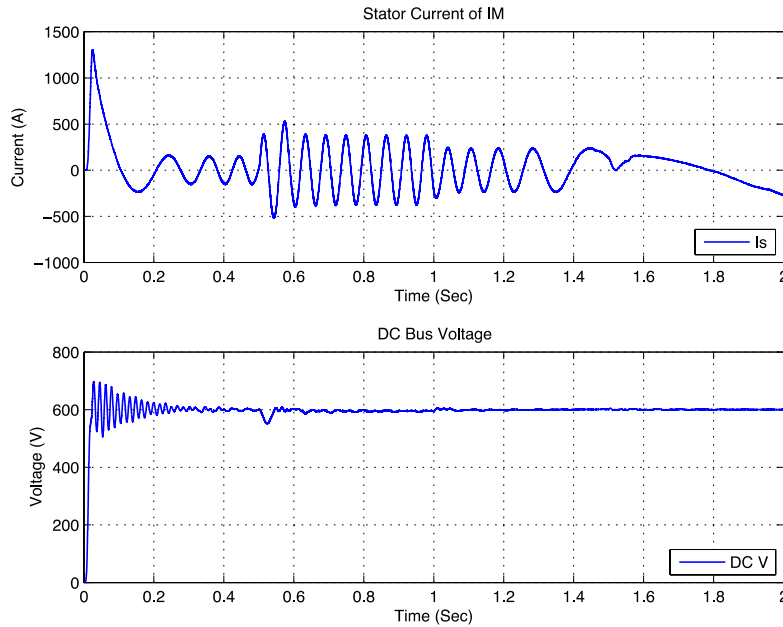


Fig. 8 Stator current and DC Bus voltage response during different operation modes.

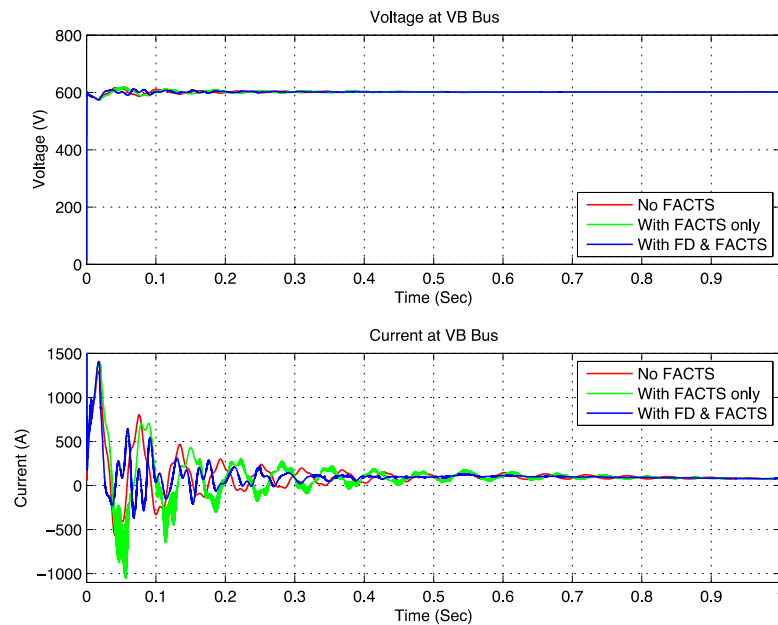


Fig. 9 Voltage and current at Battery Bus under normal condition.

International Journal of Advanced Research in Electrical, Electronics and Instrumentation Engineering

(An ISO 3297: 2007 Certified Organization)

Vol. 2, Issue12, December 2013

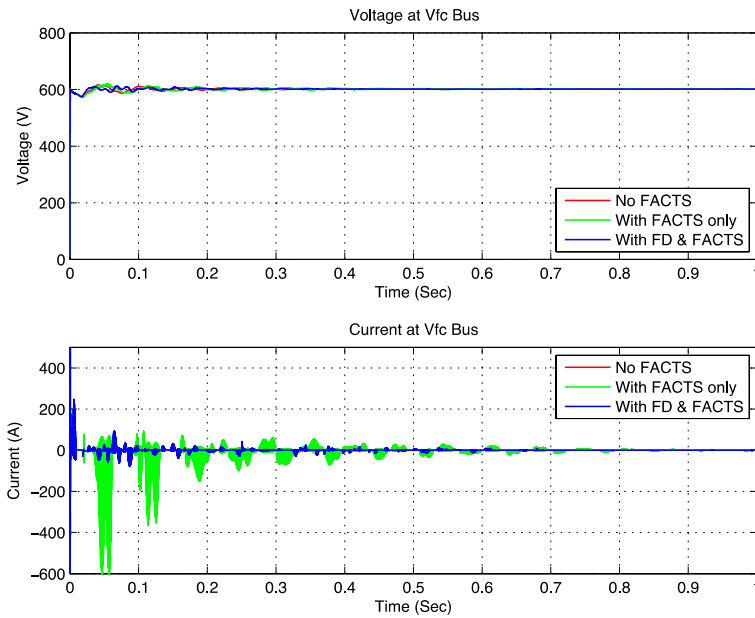


Fig. 10 Voltage and current at FCBus under normal condition.

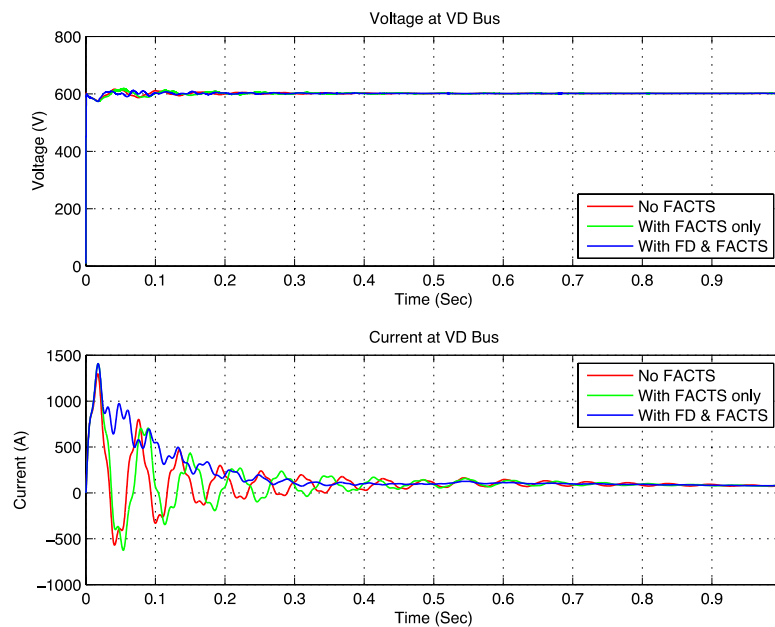


Fig. 11 Voltage and current at VDBus under normal condition.

International Journal of Advanced Research in Electrical, Electronics and Instrumentation Engineering

(An ISO 3297: 2007 Certified Organization)

Vol. 2, Issue12, December 2013

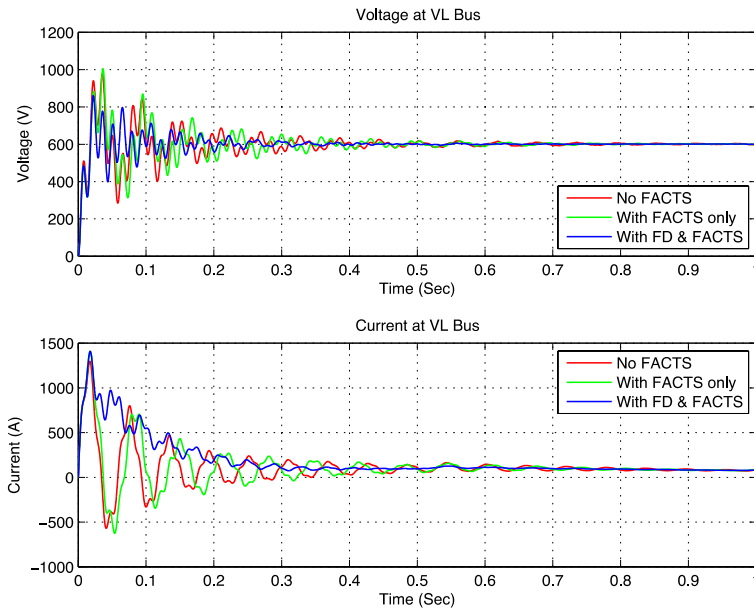


Fig. 12 Voltage and current at VLBus under normal condition.

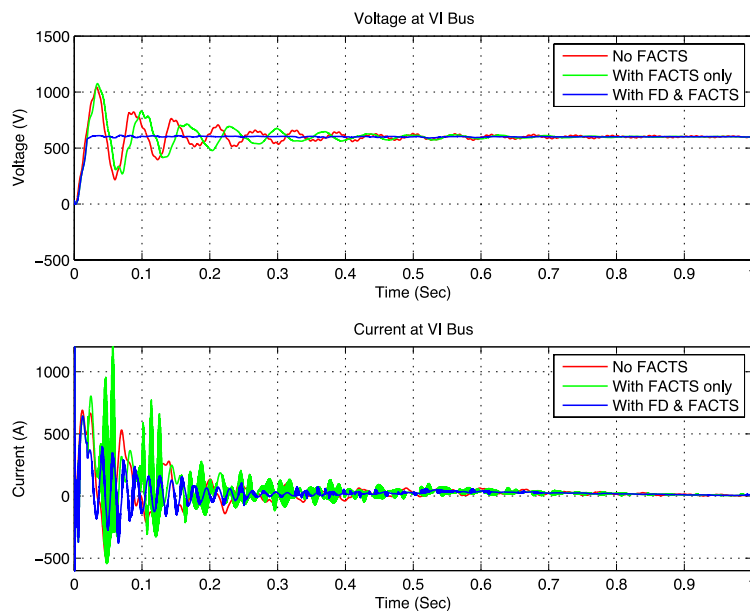


Fig. 13 Voltage and current at VIBus under normal condition.

International Journal of Advanced Research in Electrical, Electronics and Instrumentation Engineering

(An ISO 3297: 2007 Certified Organization)

Vol. 2, Issue12, December 2013

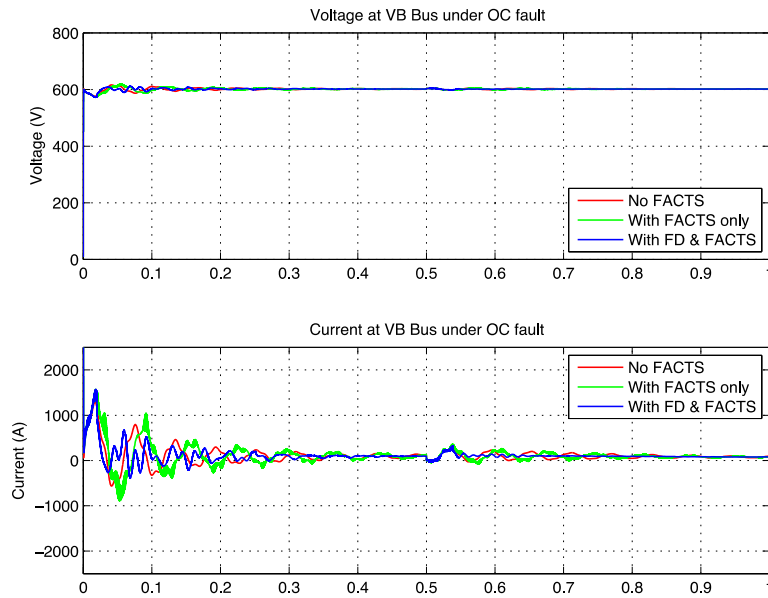


Fig. 14 Voltage and current at Battery Bus under open circuit fault condition at VD Bus.

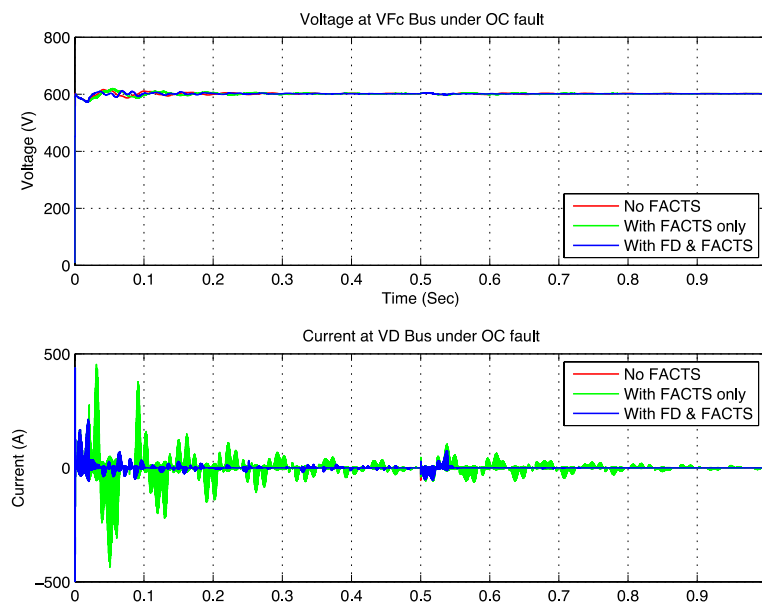


Fig. 15 Voltage and current at FCBus under open circuit fault condition at VD Bus.

International Journal of Advanced Research in Electrical, Electronics and Instrumentation Engineering

(An ISO 3297: 2007 Certified Organization)

Vol. 2, Issue12, December 2013

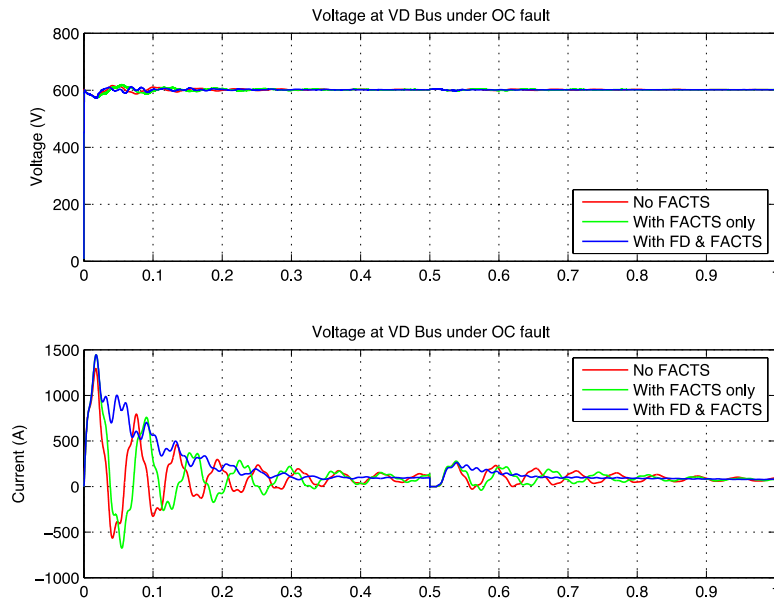


Fig. 16 Voltage and current at VDBus under open circuit fault condition at VD Bus.

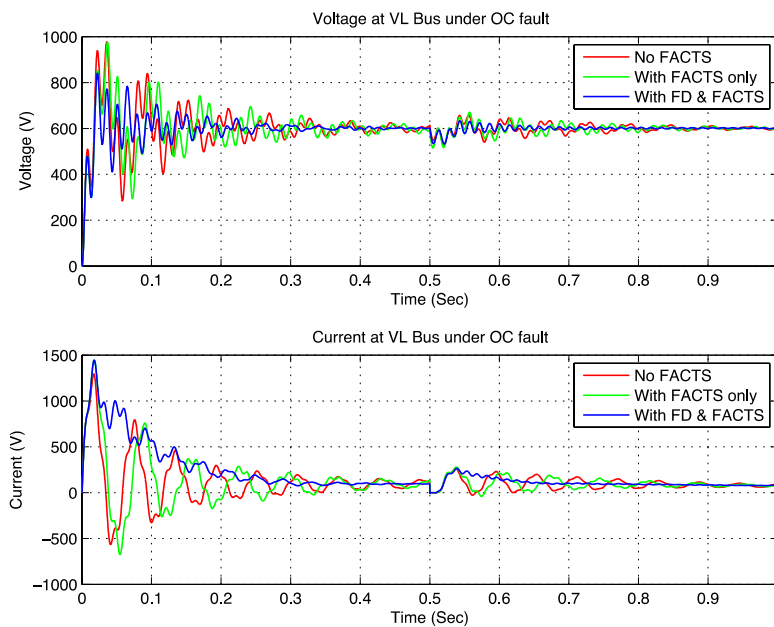


Fig. 17 Voltage and current at VLBus under open circuit fault condition at VD Bus.

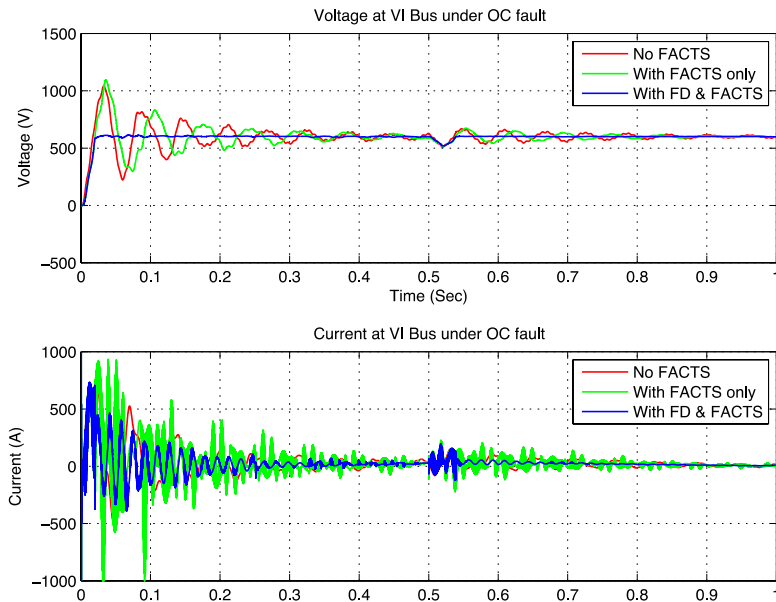


Fig. 18 Voltage and current at VIBus under open circuit fault condition at VD Bus.

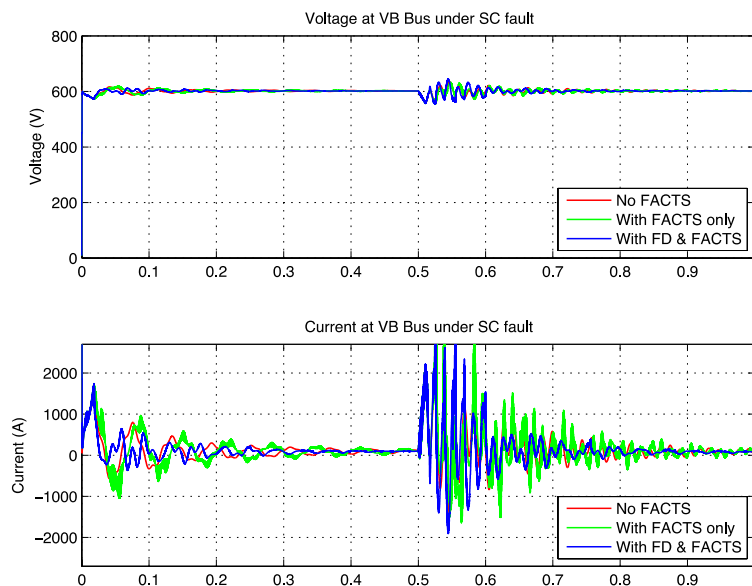


Fig. 19 Voltage and current at Battery Bus under short circuit fault condition at VD Bus.

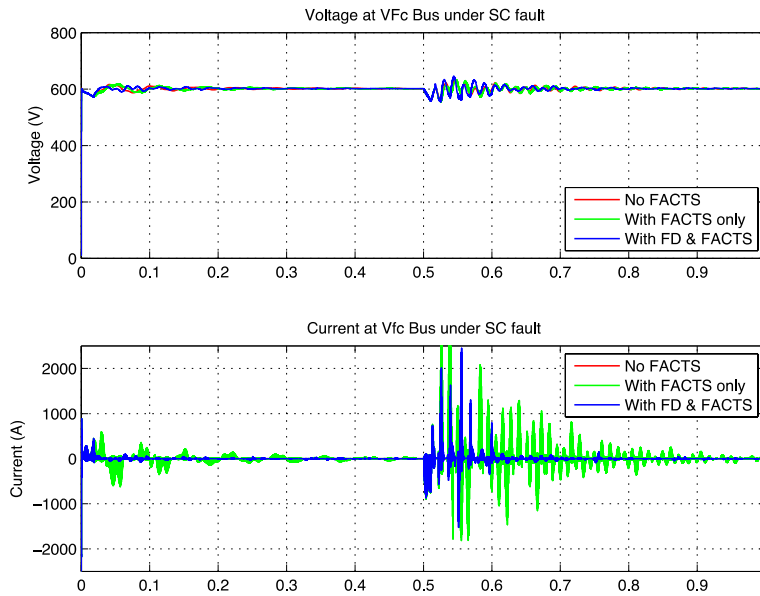


Fig. 20 Voltage and current at FCBus under short circuit fault condition at VD Bus.

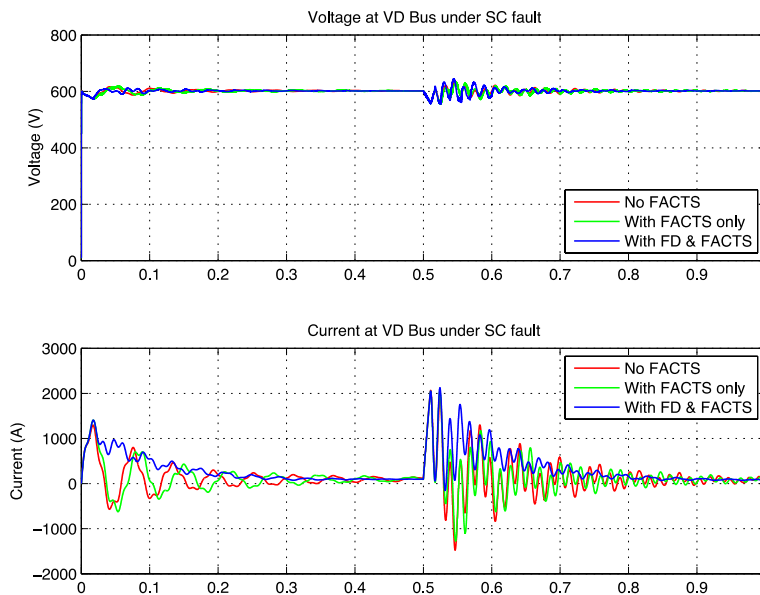


Fig. 21 Voltage and current at VDBus under short circuit fault condition at VD Bus.

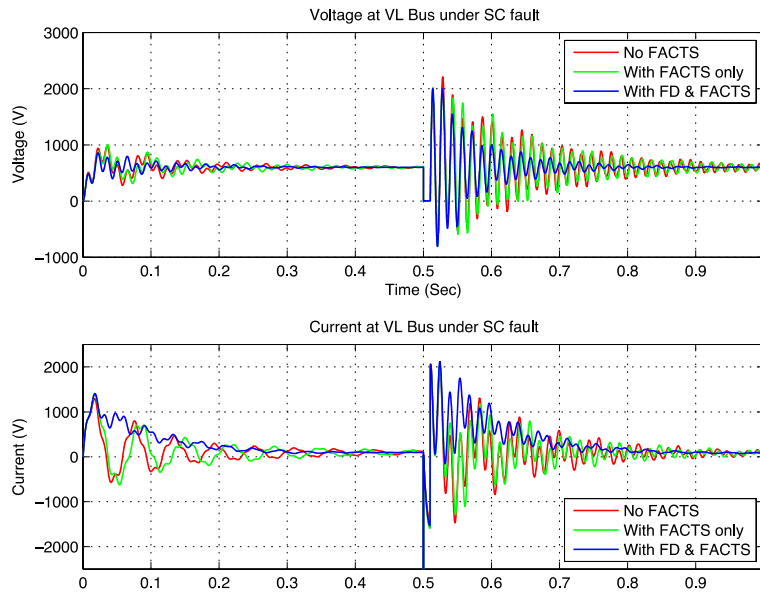


Fig. 22 Voltage and current at VLBus under short circuit fault condition at VD Bus.

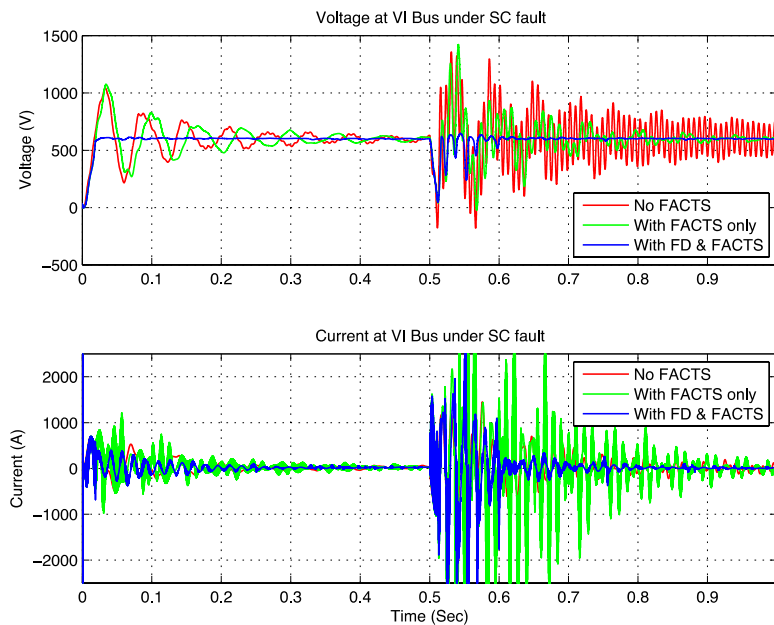


Fig. 23 Voltage and current at VIBus under short circuit fault condition at VD Bus.

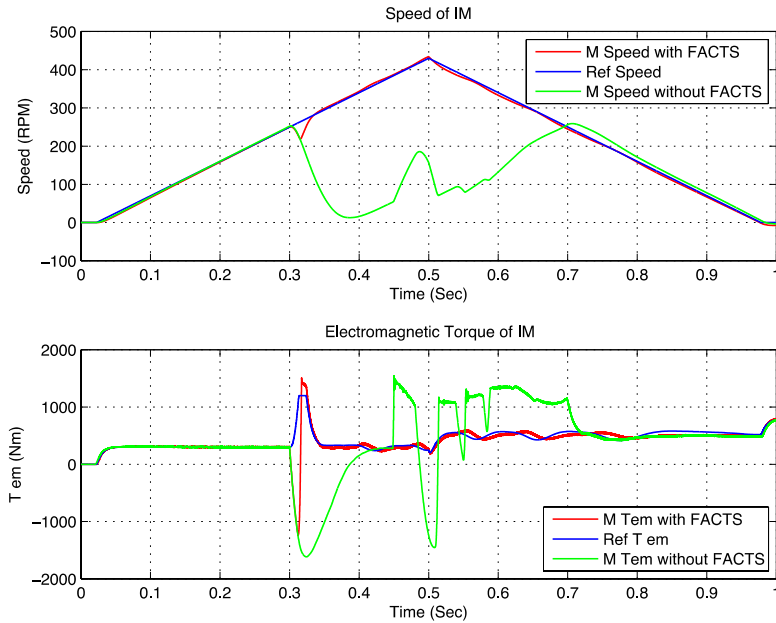


Fig. 24 Motor response during different operation modes under short circuit fault condition at AC Bus.

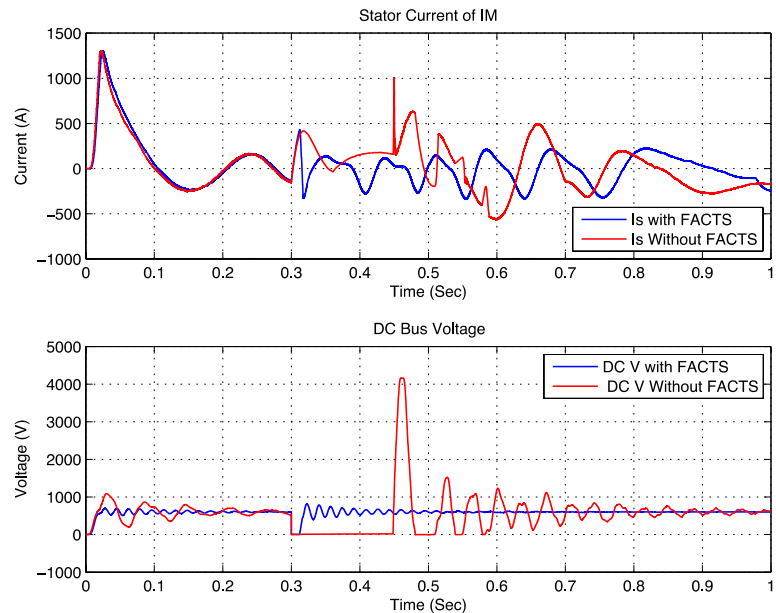


Fig. 25 Stator current and DC Bus voltage response during different operation modes under short circuit fault condition at AC Bus



International Journal of Advanced Research in Electrical, Electronics and Instrumentation Engineering

(An ISO 3297: 2007 Certified Organization)

Vol. 2, Issue 12, December 2013

V. CONCLUSIONS AND EXTENSIONS

The paper validated the new efficient switched filter compensation scheme and the error driven multi-loop control strategy to ensure minimal inrush current conditions, energy recovery via the free-wheeling diode and common DC Bus stabilization for the hybrid DC source comprising the FC and Lithium-Ion battery feeding the VSI 6-Pulse Inverter drive for the AC three-phase squirrel-cage induction motor used as the EV-propulsion system. The scheme utilizes a simple but effect series-parallel switched capacitor-filter to ensure dynamic terminal voltage stabilization, effective energy utilization under load switching and faults. The dynamic modelling and coordinated control strategy for the integrated EV drive with free-wheeling diode scheme using hybrid fuel cell and Lithium-Ion battery. The integrated DC/AC drive scheme is stabilized using low cost pulse width modulated/switched filter compensation (SFC). The objective of the multi loop regulator is to ensure a fully stabilized DC Bus voltage with reduced inrush current conditions and energy recovery under source and load excursions.

The paper also presented the validation of the multi loop modified PID controller with additional error-squared accelerated response and error-rate stabilization for the Lithium-ion battery, fuel cell scheme for EV powered four-wheel AC drive using three-phase squirrel-cage induction motors. The AC induction motor is validated for different operating conditions using the decoupled-direct torque control (DTC) technique.

The research is now extended to other AC drive systems including permanent magnet Induction motor, PM-Synchronous and Switched Reluctance motors with different SFC filter topologies and modified control strategies using dynamic PSO/Harmony Search/Bacteria foraging and adaptive soft computing evolutionary computing dynamic gain controllers.

REFERENCES

- [1] D. A. J. Rand and R. Woods, "Batteries for electric vehicles," 1981.
- [2] F. Burke, "Batteries and ultracapacitors for electric, hybrid, and fuel cell vehicles, Proceedings of the IEEE, vol. 95, no. 4, pp. 806-820, 2007.
- [3] M. Zeraoulia, M. E. H. Benbouzid, and D. Diallo, "Electric motor drive selection issues for HEV propulsion systems: A comparative study," IEEE Transactions on Vehicular Technology, vol. 55, no. 6, pp. 1756-1764, 2006.
- [4] C. Chan, "The state of the art of electric and hybrid vehicles," Proceedings of the IEEE, vol. 90, no. 2, pp. 247-275, 2002.
- [5] D. O. Neacsu and K. Rajashekara, "Comparative analysis of torque-controlled im drives with applications in electric and hybrid vehicles," IEEE Transactions on Power Electronics, vol. 16, no. 2, pp. 240-247, 2001.
- [6] M. Farasat and E. Karaman, "Speed sensorless electric vehicle propulsion system using hybrid foc-dtc induction motor drive," in International Conference on Electrical Machines and Systems (ICEMS). IEEE, pp. 1-5, 2011.
- [7] Faiz, M. B. B. Sharifian, A. Keyhani, and A. B. Proca, "Sensorless direct torque control of induction motors used in electric vehicle," IEEE Transactions on Energy Conversion, vol. 18, no. 1, pp. 1-10, 2003.
- [8] O. Ellabban, J. Van Mierlo, and P. Lataire, "Direct torque controlled space vector modulated induction motor fed by a z-source inverter for electric vehicles," in Power Engineering, Energy and Electrical Drives (POWERENG), International Conference on. IEEE, pp.1-7, 2011.
- [9] T. G. Habetler, F. Profumo, M. Pastorelli, and L. M. Tolbert, "Direct torque control of induction machines using space vector modulation," IEEE Transactions on Industry Applications, vol. 28, no. 5, pp. 1045-1053, 1992.
- [10] Takahashi and T. Noguchi, "A new quick-response and high-efficiency control strategy of an induction motor," IEEE Transactions on Industry Applications, no. 5, pp. 820-827, 1986.
- [11] M. Aware, S. Tarnekar, and J. G. Chaudhari, "Improved direct torque control induction motor drive," in TENCON 2006. IEEE Region 10 Conference. IEEE, pp. 1-4, 2006.
- [12] R. H. Daugherty and C. H. Wennerstrom, "Need for industry standards for AC induction motors intended for use with adjustable-frequency controllers," IEEE Transactions on Industry Applications, vol. 27, no. 6, pp. 1175-1185, 1991.
- [13] B. K. Bose, Modern power electronics and AC drives. Prentice hall USA, vol. 712, 2002.
- [14] Z. Xinghua, Z. Houbei, and S. Zhenxing, "Efficiency optimization of direct torque controlled induction motor drives for electric vehicles," in Electrical Machines and Systems (ICEMS), International Conference on. IEEE, pp. 1-5, 2011.
- [15] U. Choiet *et al.*, "A high efficiency drive system for electric vehicle," IEVS-13, pp. 537-543, 1996.
- [16] Matsus and S. Katsuta, "Fast rotor flux control of vector controlled induction motor operating at maximum efficiency for electric vehicles," EVS-13, p272-278, 1996.
- [17] Faiz, S. Hossieni, M. Ghaneei, A. Keyhani, and A. Proca, "Direct torque control of induction motors for electric propulsion systems," Electric power systems research, vol. 51, no. 2, pp. 95-101, 1999.
- [18] U. Baader, M. Depenbrock, and G. Gierse, "Direct self control (dsc) of inverter-fed induction machine: A basis for speed control without speed measurement," IEEE Transactions on Industry Applications, vol. 28, no. 3, pp. 581-588, 1992.
- [19] O. Kukrer, "Discrete-time current control of voltage-fed three-phase pwm inverters," IEEE Transactions on Power Electronics, vol. 11, no. 2, pp. 260-269, 1996.
- [20] P. Vas, Sensorless vector and direct torque control. Oxford university press Oxford, UK, 1998.
- [21] James and D. Andrew, "Fuel cell systems explained," John Wiley & Sons, Ltd., Chichester, 2003.